City Research Online

City, University of London Institutional Repository

Citation: Ahmad, H., Karim, M. R. & Rahman, B. M. (2019). Dispersion-engineered silicon nitride waveguides for mid-infrared supercontinuum generation covering the wavelength range 0.8-6.5 mu m. Laser Physics, 29(2), 025301. doi: 10.1088/1555-6611/aaf63d

This is the accepted version of the paper.

This version of the publication may differ from the final published version.

Permanent repository link: https://openaccess.city.ac.uk/id/eprint/21595/

Link to published version: https://doi.org/10.1088/1555-6611/aaf63d

Copyright: City Research Online aims to make research outputs of City, University of London available to a wider audience. Copyright and Moral Rights remain with the author(s) and/or copyright holders. URLs from City Research Online may be freely distributed and linked to.

Reuse: Copies of full items can be used for personal research or study, educational, or not-for-profit purposes without prior permission or charge. Provided that the authors, title and full bibliographic details are credited, a hyperlink and/or URL is given for the original metadata page and the content is not changed in any way.

City Research Online: http://openaccess.city.ac.uk/ publications@city.ac.uk

Dispersion-engineered silicon nitride waveguides for mid-infrared supercontinuum generation covering the wavelength range 0.8–6.5 μm

H. Ahmad[1,2], M. R. Karim[1] and B. M. A. Rahman[3]

[1]Photonics Research Centre, Faculty of Science, University of Malaya, 50603 Kuala Lumpur, Malaysia
[2]Visiting Professor at the Department of Physics, Faculty of Science and Technology, Airlangga University, Surabaya 60115, Indonesia
[3]Department of Electrical and Electronic Engineering, City University of London, Northampton Square, London, EC1V 0HB, UK

E-mail: harith@um.edu.my

February 2018

Abstract. We numerically demonstrate the generation of a mid-infrared supercontinuum (SC) through the design of an on-chip complementary metal oxide semiconductor (CMOS) compatible 10-mm-long air-clad rectangular waveguide made using stoichiometric silicon nitride (Si_3N_4) as the core and MgF_2 glass as its lower cladding. The proposed waveguide is optimized for pumping in both the anomalous and all-normal dispersion regimes. A number of waveguide geometries are optimized for pumping at 1.55 μm with ultrashort pulses of 50-fs duration and a peak power of 5 kW. By initially keeping the thickness constant at 0.8 μm, four different structures are engineered with varying widths between 3 μm and 6 μm. The largest SC spectral evolution covering a region of 0.8 μm to beyond 6.5 μm could be realized by a waveguide geometry with a width of 3 μm. Numerical analysis shows that increasing width beyond 3 μm by fixing thickness at 0.8 μm results in a reduction of the SC extension in the long wavelength side. However, the SC spectrum can be enhanced beyond 6.5 μm by increasing the waveguide thickness beyond 0.9 μm with the same peak power and pump source. To the best of our knowledge, this is first time report of a broad SC spectral evolution through numerical demonstration in the mid-infrared region by the silicon nitride waveguide. In the case of all-normal dispersion pumping, a flatter SC spectra can be predicted with the same power and pump pulse but with a reduced bandwidth spanning 950–2100 nm.

Keywords: Numerical analysis and approximation, Integrated optics, Ultrafast nonlinear optics, Supercontinuum generation.

1. Introduction

The generation of Supercontinuum (SC) spectra has recently attracted a lot of attention due to the formation of a very broad, continuous spectra through the application of an intense, ultrashort optical pulse into the optical waveguide [1]. Over the last decade, microstructured fiber designs have been widely employed for the design and development of high brightness SC sources capable of operating in the ultraviolet to mid-infrared region [2]. These SC sources are designed using highly nonlinear fibers and have found significant interest for various applications such as spectroscopy, optical coherence tomography, telecommunication, bio-imaging, and high precision frequency metrology [3, 4]. Typically these SC sources are designed to have long interaction lengths, which may reduce the shot-to-shot coherence of such light sources [5]. In this manner, ultrashort pulses with durations of less than 100-fs with short device lengths are more suitable for the coherence improvement of SC generation at the waveguide output [6, 7, 8]. Over the last decade, low cost, scalable integrated optical components such as nonlinear silicon photonics, which is fabricated on Silicon-On Insulator (SOI) platforms, are widely used CMOS compatible technologies among the researchers [9]. In recent years, on chip silica (SiO_2) based CMOS compatible integrated photonic devices have emerged as viable candidates for SC generation between ultraviolet (UV) and mid-infrared (MIR) regions [10, 11]. Silicon nitride (Si_3N_4) is also a well-established material which displays a broad transparency window spanning from the visible to the MIR regions. Furthermore, Si_3N_4 has also recently been seen as a highly potential candidate for the generation of octave spanning broadband SC generation as well as many other applications in the MIR regime [12]. Moreover, the optical properties of Si_3N_4 can be further exploited by the tight light confinement of on-chip integrated optical devices, which yields a strong nonlinear interaction inside the waveguide [13, 14].

Silicon (Si) has a large Kerr nonlinear parameter (n_2) which results in strong nonlinear interaction inside the optical waveguide. However, owing to a small energy band gap (1.12 ev) in most telecommunication wavelengths, it suffers from high two-photon absorption (TPA) and subsequently induces free carrier absorption which clamps the SC broadening in the MIR regime [15, 16]. On the other hand, SiO_2 suffers from high material absorption which limits the MIR region SC generation to below 2.5 μm [17]. Silicon nitride possesses a comparatively lower Kerr nonlinearity than Si but has a Kerr nonlinearity of ten times larger than that of SiO_2 [18]. Unlike Si, Si_3N_4 does not have any TPA absorption due to its large energy band gap ($\sim$ 5 ev) at 1.55 μm even at high power levels and exhibits very low linear loss which can provide a large nonlinear phase shift with a modest pump power and transparency from ultraviolet to a wavelength range of more than 6 μm [18, 19, 20, 21]. Moreover, the nonlinear Kerr parameter of Si_3N_4 can be enhanced by varying its stoichiometry, which allows high power handling capabilities that makes it attractive platform for nonlinear optics applications [22, 23]. Furthermore, due to its low Raman effect, high shot-to-shot coherence can be observed over the entire SC bandwidth obtained at the Si_3N_4 waveguide output [24]. In order to obtain SC generation with full spatial and temporal coherence, Si_3N_4 would be the more suitable material for the fabrication of on-chip CMOS compatible integrated photonic devices for various applications in the MIR region [25, 26].

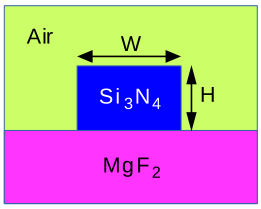

Figure 1. Waveguide geometry

Recently, several research groups have demonstrated broadband SC generation between the UV and MIR regions using Si_3N_4 waveguide [13, 14, 21, 24, 25, 26, 27]. Zhao *et al.* [13] reported an octave spanning SC generation covering a region of 488–978 nm in a 1-cm long air-clad Si_3N_4 waveguide using SiO_2 lower cladding with a 100-fs duration Ti:Sapphire laser pulse emitted at 795 nm with a peak power of 874 W. Salem *et al.* [14] experimentally demonstrated the generation of a MIR SC from 1250 nm to 2600 nm using a 2-cm long Si_3N_4 waveguide when pumped at 1920 nm using all-fiber femtosecond laser source with a peak power of 2 kW. Luke *et al.* [21] experimentally reported a MIR frequency comb spanning from 2.3 to 3.5 μm using a Si_3N_4 microresonator when pumped at 2.6 μm with a peak power of 50 W. Johnson *et al.* [24] experimentally reported 1.4 octaves SC generation spanning from 673 nm to 1944 nm in a 8-mm long rectangular Si_3N_4 waveguide when pumped at 1030 nm with pulses of 92-fs duration at a peak power of 4.75 kW. Liu *et al.* [25] demonstrated the generation of a 1.5 octaves MIR SC covering the wavelength range 820–2250 nm both experimentally and theoretically using an Er-fiber laser when pumped at 1.555 μm with pulses of 105-fs duration in a 10-mm-long Si-rich silicon nitride waveguide with a peak power of 1.33 kW. Porcel *et al.* [26] reported the generation of a MIR SC using stoichiometric Si_3N_4 from 526 nm to 2600 nm by pumping at 1.56 μm with pulses of 120-fs duration and a pulse peak

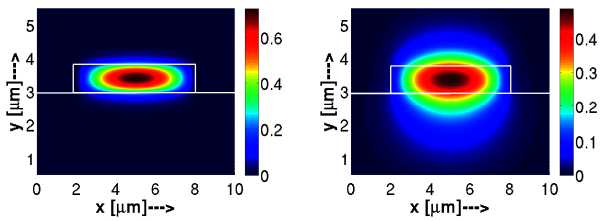

Figure 2. Field profiles (transverse cross-sectional view) of fundamental quasi-TE mode (H_y^{11}) for the rectangular Si_3N_4 channel waveguide structure with $H = 0.8$ μm, $W = 6$ μm plotted at the wavelength of (a) $\lambda = 1.55$ μm and (b) $\lambda = 4$ μm. Color bar indicates the magnitude of magnetic field distribution in A/m.

power of 117 kW. Epping *et al.* [27] reported an on-chip ultrabroadband SC generation spanning from 470 nm to 2130 nm in a CMOS compatible Si_3N_4 waveguides when pumped at a center wavelength of 1064 nm with pulses of 115-fs duration and a peak power of 42 MW.

In this work, a 10-mm-long dispersion engineered Si_3N_4 channel waveguide for the ultrabroadband MIR SC generation in both the anomalous and all-normal dispersion regimes is numerically proposed and designed. In the case of anomalous dispersion pumping, a SC spectrum spanning from 0.8 μm to beyond 6.5 μm is obtained when pumped at 1.55 μm at an input peak power of 5 kW. The SC spectrum can be broadened from 950 nm to 2100 nm with the same peak power and pump source for the case of the all-normal dispersion regime. In this case, a flatter SC spectra with a reduced bandwidth is observed compared to that obtained in the anomalous dispersion regime. It is prudent to note that in most of the aforementioned works reported earlier, researchers employed silica as a lower cladding for the design of Si_3N_4 waveguides for MIR SC generation. As silica suffers high material absorption loss in the MIR region of more than 2.3 μm and MgF_2 glass has transparency of beyond 7 μm, thus in this work we consider MgF_2 as a bottom cladding in the proposed on-chip CMOS compatible air-clad waveguide design. In recent years, researchers have employed MgF_2 glass as a cladding/buffer layer/substrate for waveguide fabrications with chalcogenide glass for several mid-infrared region applications. In this regard, we propose an air-clad Si_3N_4 waveguide design using MgF_2 glass as a bottom cladding for the generation of a broadband SC output for various sensing and imaging applications [28, 29].

2. Theory

The schematic diagram of the proposed rectangular air-clad Si_3N_4 waveguide with a MgF_2 glass lower cladding is shown in Fig. 1. During the simulation of the waveguide geometry, the linear refractive index of Si_3N_4 for the wavelength range of interest is calculated from the Sellmeier equation considered in [21]. The linear refractive index of MgF_2 glass is calculated from the Sellmeier equation given in [30]. Using in-house developed finite-element method (FEM) based full vectorial mode-solver, the mode propagation constant, $\beta(\omega)$ of the fundamental mode up to the wavelength of range of interest can be calculated with any refractive index distribution [31]. The mode effective index, n_{eff} of a fundamental mode for the proposed waveguide structure is calculated from $\beta(\omega)$. To obtain high accuracy modal solutions, the waveguide geometries are represented by 500,000 first order triangular elements (500×500 mesh) in their transverse directions. The accuracy of the developed modal solutions is tested through Aitken's extrapolation technique [32]. The convergence between the raw FEM results and the extrapolated values with an increasing number of mesh elements is obtained at the mesh divisions of 500×500 and above for the proposed silicon nitride waveguide structures, with a more detailed description given in Karim *et al.* [33]. Figure 2 shows the field profiles of the fundamental quasi-TE mode (H_y^{11}) of our proposed rectangular channel waveguide geometry with $H = 0.8$ μm and $W = 6$ μm. The field profiles of Figs. 2(a) and 2(b) are plotted at 1.55 μm and 4 μm wavelengths, respectively. The spatial field profiles of the fundamental quasi-TE mode at two different wavelengths such as short and long side exhibit very good field confinement to the central core region which induces high nonlinear interation inside the waveguide. The group-velocity dispersion (GVD), on the other hand, an another crucial waveguide characterizing parameter, is evaluated from the n_{eff} using the group-velocity dispersion equation [34] as follows:

$$D(\lambda) = -\frac{\lambda}{c}\frac{d^2 Re(n_{\text{eff}})}{d\lambda^2}, \tag{1}$$

where c indicates the speed of light in the vacuum.

The generation of a broadband MIR SC spectrum in the optimized waveguide can be studied by solving the generalized nonlinear Schrödinger equation (GNLSE) [35, 36] for single polarization in both the all-normal and anomalous dispersion regimes are given by:

$$\frac{\partial}{\partial z}A(z,T) = -\frac{\alpha}{2}A + \sum_{m\geq 2}^{14}\frac{i^{m+1}}{m!}\beta_m\frac{\partial^m A}{\partial T^m}$$
$$+i\gamma\left(|A|^2 A + \frac{i}{\omega_0}\frac{\partial}{\partial T}(|A|^2 A)\right). \tag{2}$$

In this regard, *A(z,T)* represents the pulse envelop which evolves along the entire length of the waveguide

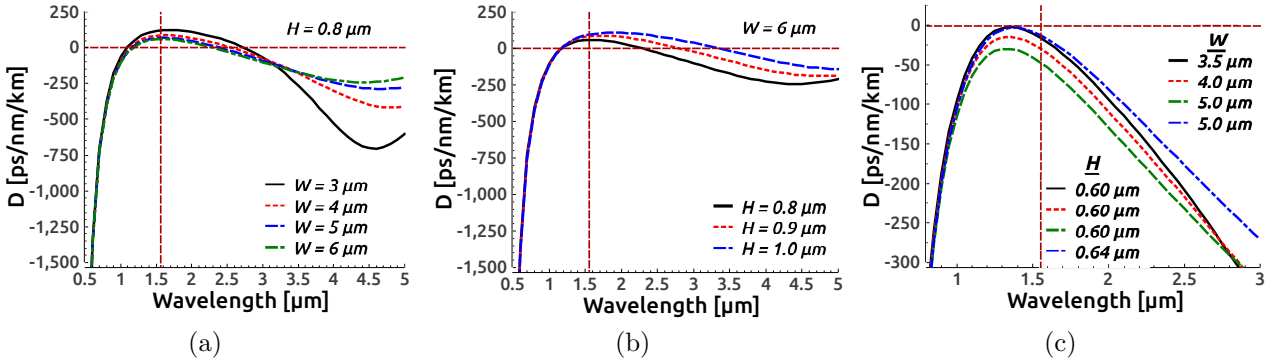

Figure 3. Three sets of GVD curves tailored for the optimized Si_3N_4 waveguide geometry proposed in Fig. 1 for pumping at 1.55 μm in (a) anomalous GVD region keeping waveguide thickness, $H = 0.8$ μm constant by varying width, W between 3 μm and 6 μm with a step of 1 μm; (b) anomalous GVD region by varying H between 0.8 μm and 1 μm with a step of 100 nm keeping W constant at 6 μm; (c) all-normal GVD region by varying H and W of the structure. Vertical dashed lines indicate pump wavelength.

structure in a retarded time frame with the reference $T = t - \beta_1 z$ moving at the group velocity $v_g = 1/\beta_1$, the parameter β_m $(m \geq 2)$ is the second and higher-order dispersion terms expanded by Taylor-series expansion from the mode propagation constant $\beta(\omega)$ around the center angular frequency ω_0 and α is the linear attenuation (propagation loss) of Si_3N_4. The nonlinear parameter is defined as $\gamma = n_2\omega_0/(cA_{\text{eff}})$, where n_2 is the nonlinear refractive index at the center (pump) frequency and $A_{\text{eff}} = (\int\int |E|^2 dxdy)^2/(\int\int |E|^4 dxdy)$ is the frequency dependent mode effective area of the fundamental mode of the waveguide structure.

3. Results and discussion

For efficient SC generation at the optical waveguide output, the GVD plays a significant role among many other factors. Optical waveguides can be engineered in both the anomalous and normal dispersion regions for UV to MIR region SC generation. To extend the SC evolution into the MIR region, a rigorous numerical investigation has been carried out to optimize the proposed waveguide structure by varying transverse dimensions H and W for pumping at 1.55 μm in both the anomalous and all-normal GVD regimes. A number of structures are engineered in the anomalous dispersion region by varying H and W to yield zero-dispersion wavelength (ZDW) in the vicinity of the pump wavelength. As the transparency of the Si_3N_4 material extends > 6 μm, the aim of this work is to design a waveguide which can produce SC spectral evolution beyond this transparency limit. For efficient SC generation and to obtain the SC expansion into the long wavelength, the pump source location should be in close to the short-wavelength ZDW to increase soliton-order which eventually expands the spectra in the long wavelength side. In Fig. 3, two sets of

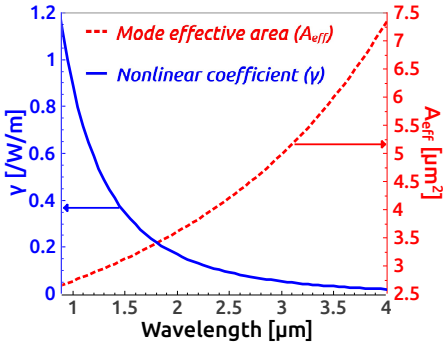

Figure 4. Variation of mode effective areas and the corresponding nonlinear coefficients of the waveguide structure, $H = 0.8$ μm, $W = 6$ μm is shown up to the wavelength range of interest.

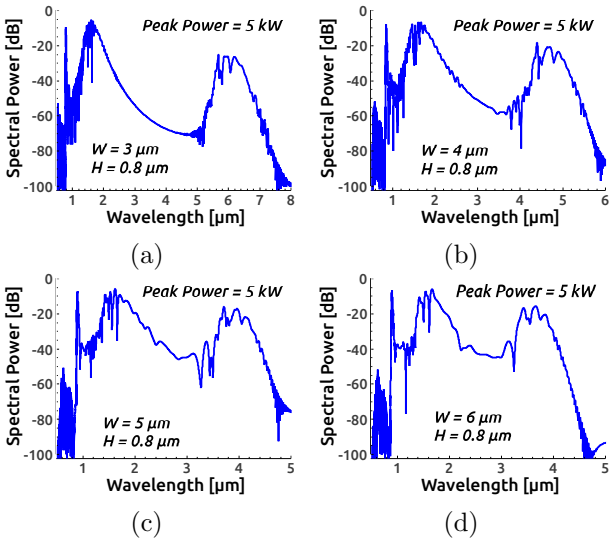

Figure 5. SC spectra at the Si_3N_4 waveguide output when pump employed in anomalous dispersion region by varying waveguide width between 3 μm and 6 μm with a step of 1 μm keeping the thickness of the waveguide constant at 0.8 μm for the largest pump peak power of 5 kW at 1.55 μm.

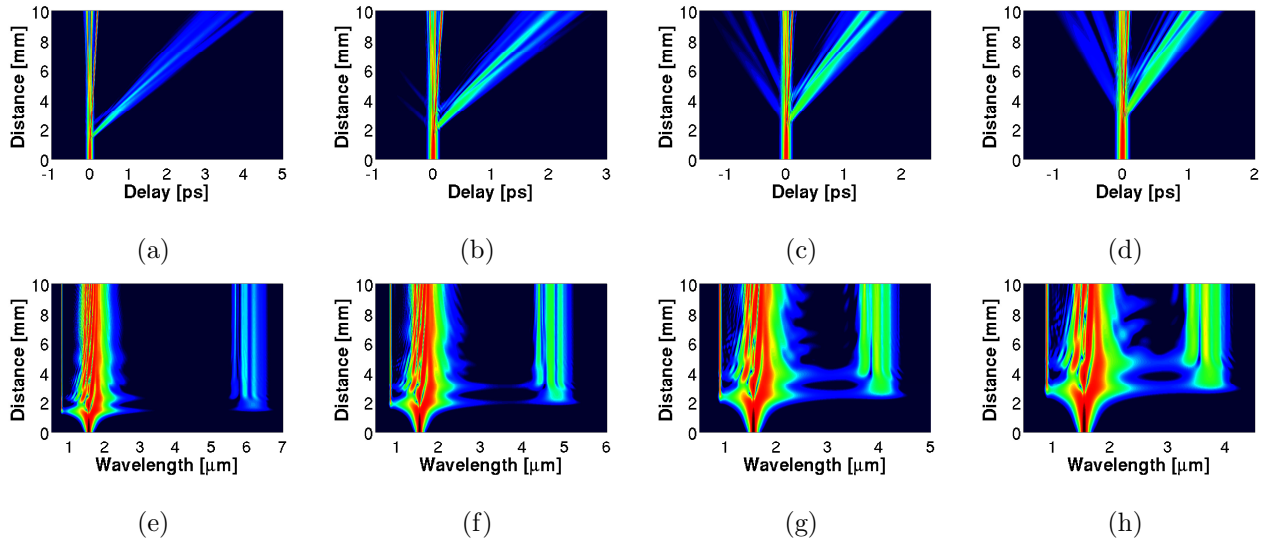

Figure 6. The temporal (top) and spectral (bottom) density evolutions in 1st, 2nd, 3rd and 4th column plotted at 1.55 μm pump wavelength corresponding to Figs. 5(a), 5(b), 5(c) and 5(d), respectively.

GVD curves are tailored for pumping the waveguide in the anomalous GVD region. For the waveguide geometry of $H = 0.8$ μm and $W = 3$ μm, the GVD parameter is calculated as 119 ps/nm/km at the pump wavelength. To obtain a GVD closer to the short-wavelength ZDW with a slightly anomalous position on the GVD curve, one of the transverse dimensions, W of the waveguide structure gradually increases from 3 μm to 6 μm with a step of 1 μm while keeping H dimension constant. With the enhancement of the waveguide width, the peak value of the each dispersion curve is seen to reduce and at the same time shifting the short-wavelength ZDW to the right as well as the long-wavelength ZDW to the left, resulting in a reduced anomalous dispersion region in subsequent designs. The lowest GVD parameter was obtained at 59 ps/nm/km for the waveguide structure with $W = 6$ μm. Fig. 3(b) gives a set of GVD curve which is dependent on the variation of the waveguide thickness with the width remaining constant during optimization. From figure, it can be observed a significant shifting of the long-wavelength ZDW to the right if the waveguide thickness is increased in a step of 100 nm which eventually yields a large anomalous dispersion regime. Enhanced GVD values at the pump wavelength with increasing thickness were also observed. Between the waveguide structural parameters H and W, it is apparent from Figs. 3(a) and 3(b) that the proposed waveguide shows highly sensitive to dispersion optimization with the variation of thickness as opposed to the variation of width for quasi-TE mode excitation.

The third set of GVD curves shown in Fig. 3(c) is tailored for all-normal dispersion SC generation by our proposed Si_3N_4 waveguide. Four geometries optimized for pumping at 1.55 μm are obtained with the all-normal dispersion GVD curves shown in Fig. 3(c) as the solid black, dotted red, dashed green and dashed-dotted blue lines, with varying the waveguide dimensional parameters, H and W. As observed in the anomalous dispersion regime, the peak of the each GVD curve, as shown in Fig. 3(c) moves downward from the zero crossing line ($D = 0$) as the width of the waveguide structures varies between 3.5 μm and 5 μm. Simultaneous variation of thickness and width for the waveguide structures with $H = 0.6$ μm or 0.64 μm and $W = 3.5$ μm or 5 μm reveals that only the right side of the GVD curve is changed (shifted) noticeably as can be seen by solid black line and dashed-dotted blue line in Fig. 3(c). Thus, a greater sensitivity to thickness as opposed to width of the waveguide is again observed.

By solving the GNLSE of Eq. (3) using symmetrized split-step Fourier method [34], the SC simulations have been carried out into our optimized Si_3N_4 waveguide by considering 2^{17} grid points. To avoid negative frequency generation in the frequency grid, the time step is chosen as 2.76-fs. The axial number of steps in the propagation direction are taken as 100,000 with a step-size of 0.1 μm. Due to the low Raman effect of the Si_3N_4 material, the GNLSE is solved without Raman term. To predict the SC generation in the proposed waveguide as well as to observe the sensitivity of the dimensional parameters of the waveguide in the SC evolution, four different structures are initially optimized for pumping at 1.55 μm by launching a TE polarized 50-fs duration full-width at half maximum (FWHM) sech pulse with a peak power of 5 kW. To predict spurious free SC spectral broadening at the

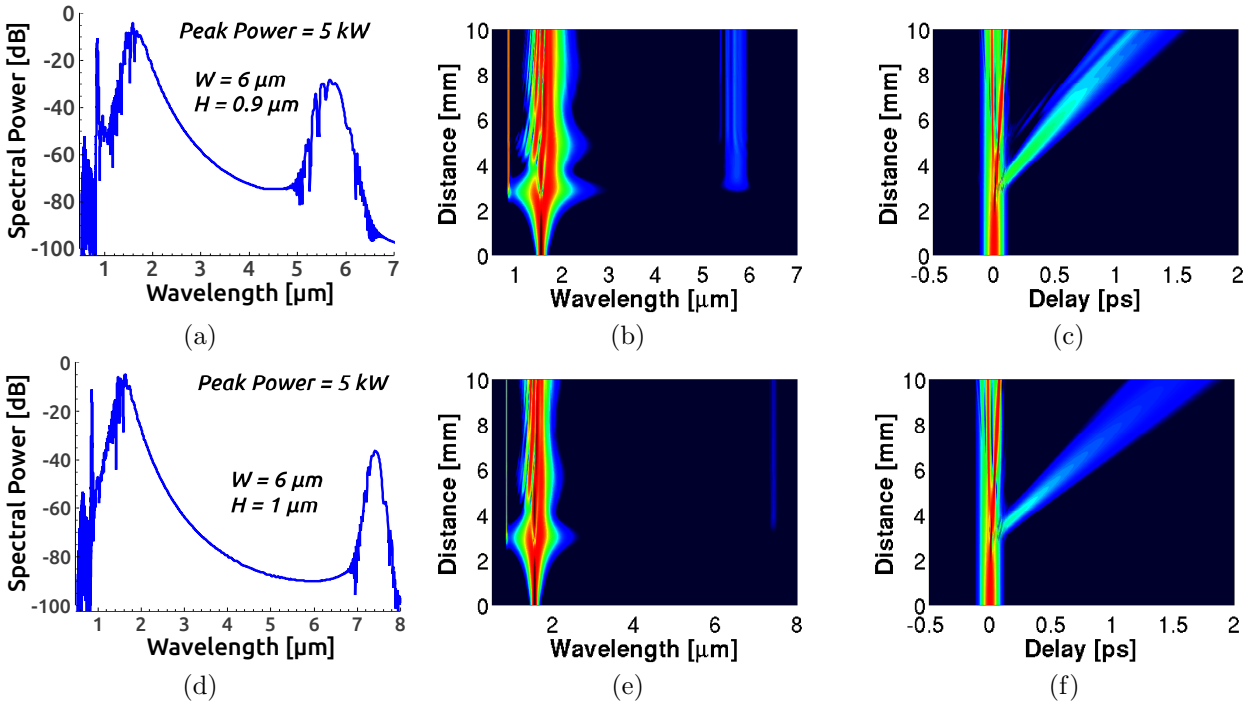

Figure 7. SC spectral evolutions for the waveguide structure containing two different thickness of 0.9 μm (top-row) and 1 μm (bottom-row) keeping width fixed at 6 μm with a peak input power of 5 kW.

waveguide output, higher-order dispersion terms up to 14^{th} order are calculated and included in all SC simulations. Mode effective areas up to the frequency range of interest are calculated for all four different structures proposed here by the FEM mode-solver and the corresponding nonlinear coefficients are evaluated, with an example illustrated in Fig. 4. The mode effective areas at the pump wavelength are calculated as 1.61 μm^2, 2.13 μm^2, 2.65 μm^2 and 3.17 μm^2 with the corresponding nonlinear coefficients of four different geometries calculated as 0.63 /W/m, 0.48 /W/m, 0.38 /W/m and 0.32 /W/m, respectively. The nonlinear parameter, n_2 and the propagation loss, α at 1.55 μm for the stoichiometric Si_3N_4 material are taken as 2.5×10^{-19} m^2/W and 0.7 dB/cm, respectively [24]. To realize an anomalous dispersion SC evolution in the MIR region, the GVD parameters are evaluated as 119 ps/nm/km, 85 ps/nm/km, 69 ps/nm/km and 59 ps/nm/km at the pump wavelength for the four optimized waveguide geometries.

Figure 5 illustrates the near-IR to MIR spectral evolution at the output of four different waveguide geometries whose GVD curves are shown in Fig. 3. Initially, the structure with dimension, $H = 0.8$ μm and $W = 3$ μm whose GVD curve is shown with solid black line in Fig. 3(a) is optimized and its corresponding spectral broadening depicts in Fig. 5(a). It can be observed from figure that SC spectrum spans up to 6.5 μm (equivalent to -30 dB level from the peak) by inducing a dip in the middle of the spectrum. The corresponding temporal and spectral density plots of Fig. 6(a) and 6(e) (extreme left column) indicate that soliton fission occurs at a distance of around 1.5 mm and four fundamental solitons are produced inside the waveguide. Due to absence of Raman scattering, no Raman induced self-frequency shift (RIFS) is produced. Owing to self-compression of applied pulses, self-phase modulation (SPM) is induced in the SC expansion around the pump wavelength. Two dispersive waves (DWs) in the short and long wavelength side of the spectrum are induced owing to the presence of two ZDWs in its corresponding GVD curve. The peak of the first DW is observed at around 900 nm and the center of the long-wavelength DW is located around at 6.2 μm. The short-wavelength phase-matched narrow band resonant DW is induced in the normal dispersion region as a result of the shedding of energy by the Raman solitons. This is a result of the presence of higher-order dispersion. As solitons are stopped at the long-wavelength ZDW, a red-shifted nonsolitonic DW is induced in the stoke-side owing to the spectral recoil effect [42].

In order to observe the width sensitivity in the SC spectrum broadening at the waveguide output, the next three geometries are optimized by varying their W between 4 μm and 6 μm while keeping H the same at 0.8 μm. It is apparent from Figs. 5(b), 5(c) and 5(d) that in these subsequent designs, the dip

induced at the middle of the spectrum is improved significantly by increasing of the waveguide width. As from the dispersion tailoring of the waveguide, increasing the width results in a smaller anomalous GVD region which decreases spectral extension at the long wavelength side yielding a reduced SC bandwidth at the waveguide output than earlier design. The SC spanning measured at -30 dB level for these three structures are 0.8–5.2 μm, 0.8–4.5 μm and 0.8–4.1 μm, respectively. From the obtained SC, it is subsequently observed that the long wavelength extension of the SC spectrum at the waveguide output depends on the location of long-wavelength ZDW and the SC spectrum becoming shorter as a result of the anomalous dispersion region narrowing for a corresponding waveguide geometries. As the position of short-wavelength ZDWs of the proposed geometries do not vary much, their corresponding DWs, which are induced in the normal dispersion region before the short-wavelength ZDWs, are observed at nearly the same locations of the spectrum for all designs. The 2nd, 3rd and 4th columns of Fig. 6 illustrates their corresponding temporal and spectral density plots, respectively. Since the proposed waveguides are asymmetric, the cut-off wavelength is obtained at around 6 μm for the waveguide geometry with W = 3 μm and for the remaining designs, the cut-off occurs beyond the 6 μm.

To test the waveguide thickness sensitivity in SC broadening, two more waveguide structures are optimized by increasing H between 0.9 μm and 1 μm while keeping their W constant at 6 μm. The corresponding GVD curves for these structures are shown as the red-dotted line and blue-dashed line of Fig. 3(b). Fig. 7 depicts the obtained SC simulations results in which the SC spectrum can be extended beyond 7.5 μm with the same low peak power of 5 kW.

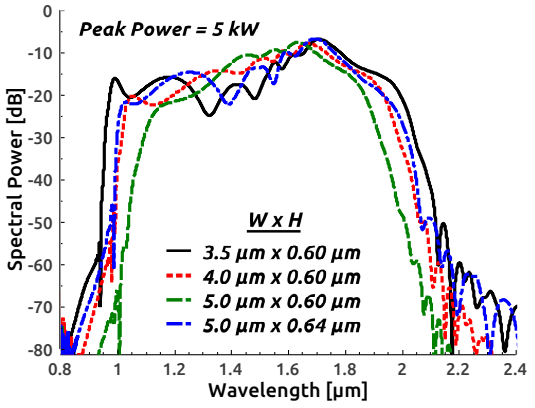

Figure 8. SC spectral evolution for four-different optimized Si_3N_4 waveguide structures whose GVD curves are shown in Fig. 3(c) pumped at 1.55 μm in all-normal dispersion region with an input peak power of 5 kW.

Similar to earlier designs, two DWs are observed in the short and long wavelength side of the spectrum. The peak of the first DW is observed at around at 0.9 μm for both designs, while Fig. 7(a) and Fig. 7(d) show that the center frequency of 2nd DW is located around at 5.8 μm and 7.5 μm, respectively. This phenomenon can clearly be observed from the spectral (middle column) and temporal (right column) density evolutions shown in Fig. 7 as well. Although increasing H results in a longer wavelength expansion, however, it induces a more spectral dip which depletes the power among the wavelength components located around the middle of the spectra. From the above analysis, it is observed that SC becomes shorter as a result of the anomalous dispersion region narrowing with the increasing of the waveguide width. On the other hand, a broad anomalous dispersion produces a wider spectra as a result of the increasing waveguide thickness.

To observe all-normal dispersion SC generation in the proposed Si_3N_4 waveguide with the MgF_2 glass based lower cladding, four different waveguide geometries are optimized by varying H and W structural parameters, with Fig. 3(c) illustrating the corresponding tailored GVD curves. To obtain a smooth and a flat spectrum, the pump wavelength should be located vicinity to the minimum dispersion (peak) of the GVD curve [43, 44]. In all the optimized waveguides, due to material composition of the waveguide structure, the pump wavelength is located to the right side of the peak of each GVD curves as can be seen in Fig. 3(c). Fig. 8 illustrates the all-normal dispersion SC generation for the waveguide geometries optimized for pumping at 1.55 μm with the largest input peak power of 5 kW and the corresponding temporal and spectral density evolutions depicted in Fig. 9. Among these structures, the largest SC extension obtained covers the wavelength range 950–2100 nm (>1 octave) which is measured at a level of -30 dB with a waveguide structure, H = 0.6 μm and W = 3.5 μm. For remaining geometries, the SC spectra becomes narrower as W becomes wider which yields a flatter spectra for the same pump peak power. There is a noticeable asymmetry observed among the spectral components located either sides of the pump wavelength. Power distribution among the spectral components whether would be uniform depending on two factors such as the shape of GVD curve and the location of a pump source wavelength. As the GVD curves are not symmetric from their peak values, the spectral power is not evenly distributed among all wavelength components in the spectrum, instead depending on the location of the pump source, either to the left, center or right side of the peak of the GVD curve. Using a pump source at a minimum dispersion (peak of GVD Curve) would give a uniform spectral

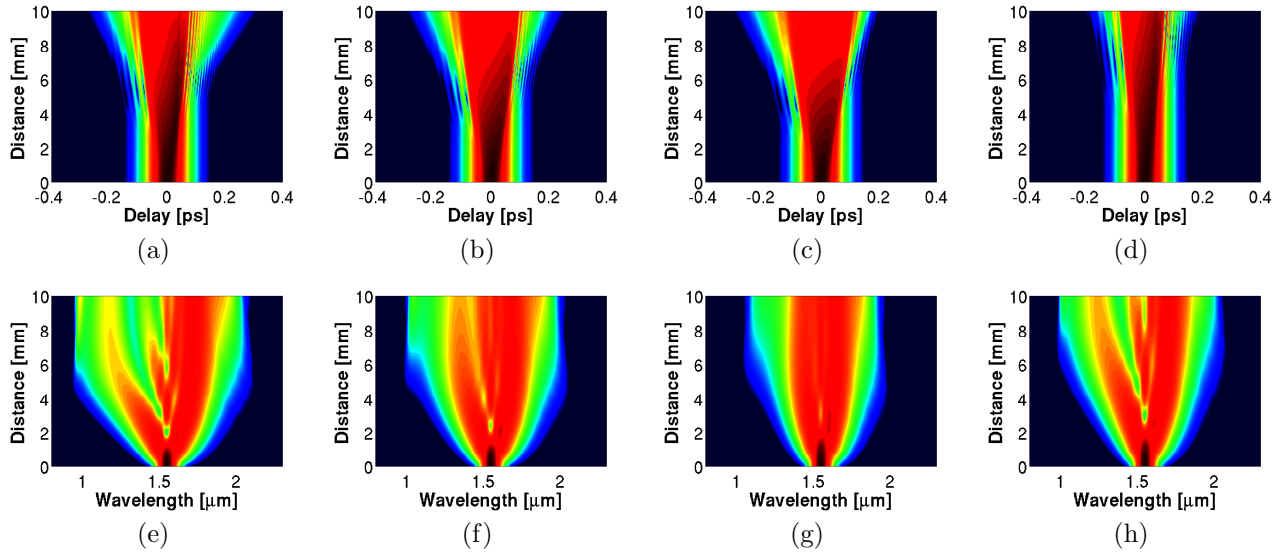

Figure 9. Spectral and temporal density evolutions correspond to the Fig. 8 of the waveguide geometry (a) & (e) $H = 0.6$ μm, $W = 3.5$ μm; (b) & (f) $H = 0.6$ μm, $W = 4$ μm; (c) & (g) $H = 0.6$ μm, $W = 5$ μm and; (d) & (h) $H = 0.64$ μm, $W = 5$ μm, respectively.

power distribution between the spectral components located either sides of the pump source. For the proposed all-normal dispersion designs, as the pump source is chosen at 1.55 μm which is located on the right side of the peak of the GVD curves, the spectral components contain more power that are located on the right side of the spectra. The spectral and temporal density evolutions in Fig. 9 are plotted against the SC spectra obtained in Fig. 8 in the all-normal dispersion region for the proposed structures to show how the SC spectrum evolves along the length of the optimized 10-mm-long Si_3N_4 waveguide. Initially, the SC spectra expands symmetrically owing to SPM between either sides of the pump wavelength and later in optical wave breaking is responsible for producing two side-lobes in the short and long wavelength sides as seen in Fig. 9 in an all-normal dispersion SC evolution.

Although SC generation in the all-normal dispersion does not show a significant MIR broadening which can easily be achieved by using silica as upper and lower claddings during the Si_3N_4 waveguide design, further MIR region spectral broadening using MgF_2 as a lower cladding of this waveguide can be realized by shifting the pump from 1.55 μm to a longer wavelength depending on the availability of the pump source. In the case of the silica based waveguide design, SC spectral broadening in the MIR will be limited owing to high material absorption of silica after 2.3 μm, however, MIR cladding absorption may not be a severe problem for a Si_3N_4 waveguide designed using MgF_2 glass as a bottom cladding.

The Si_3N_4 waveguide can be fabricated by employing two different deposition techniques such as low pressure chemical vapor deposition technique (LPCVD) and plasma enhanced vapor deposition technique (PECVD) [26, 37, 38, 39, 40]. Although the stoichiometry variation of the Si_3N_4 film provides an additional degree of freedom in waveguide fabrication, the high film stress of this material prevents the waveguide fabrication with a thickness more than 400 nm resulting in cracks formation on the Si_3N_4 film [38]. Epping *et al.* [41] reported a novel technique which uses LPCVD to produce a stress and crack free film for fabricating an optical waveguide using stoichiometric Si_3N_4 with thickness more than 9 μm. Using this technique, the proposed waveguide can be fabricated without stress and crack formation using MgF_2 as a bottom cladding. To obtain a broad area anomalous dispersion region GVD curve, the waveguide needs to be engineered with thicker dimension which helps to generate a broadband SC by the Si_3N_4 waveguide.

4. Conclusion

In this study, an on-chip CMOS-compatible novel design using stoichiometric Si_3N_4 material for a broadband SC generation is numerically proposed and demonstrated. A 10-mm-long air-clad rectangular waveguide with a Si_3N_4 as a core and MgF_2 glass as a lower cladding is optimized for pumping at 1.55 μm by varying its H and W dimensional parameters. In this study, a number of Si_3N_4 waveguide geometries for both anomalous and normal dispersion pumping have been tested by varying their H and W and examples which are suitable for SC evolutions extending from near-IR to MIR are presented here for the first time to the best of the author's knowledge. Using a low

peak power of 5 kW, a SC can be obtained spanning up to 6.5 μm with the proposed dispersion-engineered optimized structure of $H = 0.8$ μm and $W = 3$ μm. Further increasing the width results a reduction of the SC bandwidth at the waveguide output. There should be a trade off between SC bandwidth and waveguide width because the coupling of light through the pump source into the proposed waveguide would be difficult owing to the large aspect ratio. Spectral broadening can be enhanced beyond 6.5 μm (>3 octave) with the same peak power by increasing the thickness beyond 0.9 μm while keeping the waveguide width constant at 6 μm. Thus, it is apparent from the rigorous numerical analysis that MIR SC spectral broadening from 0.8 μm to beyond 6.5 μm could be realized through the thickness variations between 0.8 and 0.9 μm and width variations between 3 and 6 μm with the largest low input peak power of 5 kW. To the best of our knowledge, this is the broadest SC spectral output through numerically demonstrated in the MIR region by the Si_3N_4 waveguide reported so far.

In all-normal dispersion pumping, a SC spectral evolution covering the wavelength range 950–2100 nm (>1 octave) is obtained with the same pump and pump peak power by the structure of $H = 0.6$ μm and $W = 3.5$ μm which is optimized among four Si_3N_4 waveguide geometries. While the SC bandwidth obtained in the all-normal dispersion pumping is less than the bandwidth yielded in the anomalous dispersion regime, unlike anomalous dispersion region pumping, a flatter SC spectra can be obtained in the all-normal dispersion region owing to the absence of solitonic propagation. Employing a pump source in a longer wavelength region beyond 1.55 μm can predict a wider all-normal dispersion SC spectrum in the MIR region.

5. ACKNOWLEDGEMENT

Funding for this research was provided by the Ministry of Higher Education (MOHE) under the grants GA 010-2014 (ULUNG) and the University of Malaya under the grants RP029B-15 AFR and RU001-2017.

References

[1] Dudley J M, Genty G, and Coen S 2006 Supercontinuum generation in photonic crystal fiber *Rev. Mod. Phys.* **78** 1135–84

[2] Dudley J M and Taylor J R 2009 Ten years of nonlinear optics in photonic crystal fiber *Nat. Photonics* **3** 85–90

[3] Wei C, Zhu X, Norwood R A, Sengv F, and Peyghambarian N 2013 Numerical investigation on high power mid-infrared supercontinuum fiber lasers pumped at 3 μm *Opt. Express* **21** 29488–504

[4] Liu L, Cheng T, Nagasaka K, Tong H, Qin G, Suzuki T, and Ohishi Y 2016 Coherent mid-infrared supercontinuum generation in all-solid chalcogenide microstructured fibers with all-normal dispersion *Opt. Lett.* **41** 392–95

[5] Corwin K L, Newbury N R, Dudley J M, Coen S, Diddams S A, Weber K, and Windeler R S 2003 Fundamental Noise Limitations to Supercontinuum Generation in Microstructure Fiber *Phys. Rev. Lett.* **90** 113904

[6] Heidt A M 2010 Pulse preserving flat-top supercontinuum generation in all-normal dispersion photonic crystal fibers *J. Opt. Soc. Am. B* **27** 550–9

[7] Hu H, Li W, Dutta N K 2014 Dispersion-engineered tapered planar waveguide for coherent supercontinuum generation *Opt. Commun.* **324** 252–7

[8] Hooper L E, Mosley P J, Muir A C, Wadsworth W J, and Knight J C 2011 Coherent supercontinuum generation in photonic crystal fiber with all-normal group velocity dispersion *Opt. Express* **19** 4902–7

[9] Kuyken B, Leo F, Clemmen S, Dave U, Laer R V, Ideguchi T, Zhao H, Liu H, Safioui J, Coen S, Gorza S P, Selvaraja S K, Massar S, Osgood R M Jr., Verheyen P, Campenhout J V, Baets R, Green W M J, Roelkens G 2016 Nonlinear optical interactions in silicon waveguides *Nanophotonics* **5** 1–16

[10] Oh D Y, Sell D, Lee H, Yang K Y, Diddams S A, and Vahala K J 2014 Supercontinuum generation in an on-chip silica waveguide *Opt. Lett.* **39** 1046–8

[11] Duchesne D, Peccianti M, Lamont M R E, Ferrera M, Razzari L, Legare F, Morandotti R, Chu S, Little B E, and Moss D J 2010 Supercontinuum generation in a high index doped silica glass spiral waveguide *Opt. Express* **18** 923-30

[12] Kruckel C J, Fulop A, Ye Z, Andrekson P A, and Torres-Company V 2017 Optical bandgap engineering in nonlinear silicon nitride waveguides *Opt. Express* **25** 15370-15380

[13] Zhao H, Kuyken B, Clemmen S, Leo F, Subramanian A, Dhakal A, Helin P, Severi S, Brainis E, Roelkens G, and Baets R 2015 Visible-to-near-infrared octave spanning supercontinuum generation in a silicon nitride waveguide *Opt. Lett.* **40** 2177–80

[14] Salem R, Okawachi Y, Yu M, Lamont M, Luke K, Fendel P, Lipson M, and Gaeta A L 2015 Octave-spanning supercontinuum generation in a silicon nitride waveguide pumped by a femtosecond fiber laser at 1.9 μm in CLEO: 2015, OSA Technical Digest (online) (Optical Society of America) paper STu1I.7

[15] Hsieh I W, Chen X G, Liu X P, Dadap J I, Panoiu N C, Chou C Y, Xia F N, Green W M, Vlasov Y A, and Osgood R M, Jr. 2007 Supercontinuum generation in silicon photonic wires *Opt. Express* **15**(23) 15242–49

[16] Moss D J, Morandotti R, Gaeta A L and Lipson M 2013 New CMOS-compatible platforms based on silicon nitride and Hydex for nonlinear optics *Nat. Phtotnics* **7** 597-607

[17] Hu J, Menyuk C R, Shaw L B, Sanghera J S, and Aggarwal I D 2010 Maximizing the bandwidth of supercontinuum generation in As_2Se_3 chalcogenide fibers *Opt. Express* **18**(3) 6722–39

[18] Liu X, Zhou B, Bache M, Kruckel C J, Fulop A, Torres-Company V 2016 Octave-spanning supercontinuum generation in a silicon-rich nitride waveguide," in CLEO: OSA Technical Digest (online) (Optical Society of America), paper SW1Q.3

[19] Tan D T H, Ikeda K, Sun P C, and Fainman Y 2010 Group velocity dispersion and self phase modulation in silicon nitride waveguides *Appl. Phy. Lett.* **96** 061101

[20] Lacava C, Stankovic S, Khokhar A Z, Bucio T D, Gardes F Y, Reed G T, Richardson D J and Petropoulos P 2017 Si-rich Silicon Nitride for Nonlinear Signal Processing Applications *Sci. Reports* **7** 22

[21] Luke K, Okawachi Y, Lamont M R E, Gaeta A L, and Lipson M 2015 Broadband mid-infrared frequency comb generation in a Si_3N_4 microresonator *Opt. Lett.* **40** 4823–

26
[22] Dizaji M R, Kruckel C J, Fulop A, Andrekson P A, Torres-Company V, and Chen L R 2017 Silicon-rich nitride waveguides for ultra-broadband nonlinear signal processing *Opt. Express* **25** 12100–8
[23] Kruckel C J, Fulop A, Klintberg T, Bengtsson J, Andrekson P A, and Torres-Company V 2015 Linear and nonlinear characterization of low-stress high-confinement silicon-rich nitride waveguides *Opt. Express* **23** 25827–37
[24] Johnson A R, Mayer A S, Klenner A, Luke K, Lamb E S, Lamont M R E, Joshi C, Okawachi Y, Wise F W, Lipson M, Keller U, and Gaeta A L 2015 Octave-spanning coherent supercontinuum generation in a silicon nitride waveguide *Opt. Lett.* **40** 5117–20
[25] Liu X, Pu M, Zhou B, Kruckel C J, Fulop A, Torres-Company V, and Bache M 2016 Octave-spanning supercontinuum generation in a silicon-rich nitride waveguide *Opt. Lett.* **41** 2719–22
[26] Porcel M A G, Schepers F, Epping J P, Hellwig T, Hoekman M, Heideman R G, Van der Slot P J M, Lee C J, Schmidt R, Bratschitsch R, Fallnich C, and Boller K J 2017 Two-octave spanning supercontinuum generation in stoichiometric silicon nitride waveguides pumped at telecom wavelengths *Opt. Express* **25** 1542–54
[27] Epping J P, Hellwig T, Hoekman M, Mateman R, Leinse A, Heideman R G, Rees A, Slot P J M, Lee C J, Fallnich C, and Boller K -J 2015 On-chip visible-to-infrared supercontinuum generation with more than 495 THz spectral bandwidth *Opt. Express* **23**(15) 19596–604
[28] Yu Y, Gai X, Wang T, Ma P, Wang R, Yang Z, Choi D, Madden S, and Luther-Davies B 2013 Mid-infrared supercontinuum generation in chalcogenides *Opt. Express* **3**(8), 1075–86
[29] Chen Q, Wang X, Madsen 2012 Phase-matching and parametric conversion fro the mid-infrared in As_2S_3 waveguides *Opt. and Photon. Journal* **2** 260-4
[30] Bass M, Li G, and Stryland E V 2010 *Hand Book of Optics Vol-IV 3rd ed.* (The McGraw-Hill, New York)
[31] Rahman B M A and Davies J B 1984 Finite-element solution of integrated optical waveguides *J. Lightw. Technol.* **2** 682–8
[32] Rahman B M A and Davies J B 1985 Vector-H finite element solution of GaAs/GaAlAs rib waveguides *Procs. of IEE* **132**(6), 349–53
[33] Karim M R, Rahman B M A, and Agrawal G P 2014 Dispersion engineered $Ge_{11.5}As_{24}Se_{64.5}$ nanowire for supercontinuum generation: A parametric study *Opt. Express* **22**(25), 31029–40
[34] Agrawal G P 2013 *Nonlinear Fiber Optics 5th ed.* (Academic, San Diego, California)
[35] Karim M R, Rahman B M A, and Agrawal G P 2015 Mid-infrared supercontinuum generation using dispersion-engineered $Ge_{11.5}As_{24}Se_{64.5}$ chalcogenide channel waveguide *Opt. Express* **23** 6903–14
[36] Gai X, Madden S, Choi D Y, Bulla D, and Luther-Davies B 2010 Dispersion engineered $Ge_{11.5}As_{24}Se_{64.5}$ nanowires with a nonlinear parameter of 136 $W^{-1}m^{-1}$ at 1550 nm *Opt. Express* **18** 18866–74
[37] Hosseinnia A H, Atabaki A H, Eftekhar A A, and Adibi A 2015 High-quality silicon on silicon nitride integrated optical platform with an octave-spanning adiabatic interlayer coupler *Opt. Express* **23** 30297–307
[38] Luke K, Dutt A, Poitras C B, and Lipson M 2013 Overcoming Si_3N_4 film stress limitations for high quality factor ring resonators *Opt. Express* **21** 22829–33
[39] Boggio J M C, Monux A O, Modotto D, Fremberg T, Bodenmuller D, Giannone D, Roth M M, Hansson T, Wabnitz S, Silvestre E, and Zimmermann L 2016 Dispersion-optimized multicladding silicon nitride waveguides for nonlinear frequency generation from ultraviolet to mid-infrared *J. Opt. Soc. Am. B* **33** 2402–13
[40] Grassani D, Billat A, Pfeiffer M H P, Guo H, North T, Kippenberg T J, and Bres C S 2016 Mid-infrared supercontinuum generation in a SiN waveguide pumped at 1.55 micron in "Frontiers in Optics 2016" (Optical Society of America) p. FTu5D.3.
[41] Epping J P, Hoekman M, Mateman R, Leinse A, Heideman R G, Rees A, Slot P J M, Lee C J, and Boller K -J 2015 High confinement, high yield Si_3N_4 waveguides for nonlinear optical applications *Opt. Express* **23**(2) 642-8
[42] Biancalana F, Skryabin D V, and Yulin A V 2004 Theory of the soliton self-frequency shift compensation by resonant radiation in photonic crystal fibers, *Physical Review E* **70** 016615
[43] Karim M R, Ahmad H, and Rahman B M A 2017 All-normal dispersion chalcogenide waveguides for ultraflat supercontinuum generation in the mid-infrared region, *IEEE J. Quan. Elect.* **53**(2) 7100106
[44] Karim M R, Ahmad H, and Rahman B M A 2017 All-normal dispersion chalcogenide PCF for ultraflat mid-infrared supercontinuum generation, *IEEE Photonics Technol. Lett.* **29**(21) 1792–5